Available online at www.sciencedirect.com
SCIENCE DIRECT®
Journal of Controlled Release 92 (2003) 275–289
journal of controlled release
www.elsevier.com/locate/jconrel

Theoretical and experimental study on theophylline release from stearic acid cylindrical delivery systems

Mario Grassi[a,*], Dario Voinovich[b], Erica Franceschinis[b], Beatrice Perissutti[b], Jelena Filipovic-Grcic[c]

[a] *Department of Chemical, Environment and Raw Materials Engineering, DICAMP, University of Trieste, P. le Europa 1, 34127 Trieste, Italy*
[b] *Department of Pharmaceutical Sciences, University of Trieste, P. le Europa 1, 34127 Trieste, Italy*
[c] *Department of Pharmaceutics, Faculty of Pharmacy and Biochemistry, University of Zagreb, A. Kovačića, 10000 Zagreb, Croatia*

Received 26 February 2003; accepted 4 July 2003

Abstract

The purpose of this study is to evaluate the possibility of developing a cylindrical sustained-release dosage form for theophylline directly by means of a ram extrusion process. In particular, the formulations contained: stearic acid as a low melting binder, monohydrate lactose and polyethylene glycol 6000 as hydrophilic fillers. The influence of type and percentage of the components was studied considering different parameters such as the time required for 50% of the drug release ($t_{50\%}$)and the drug diffusion coefficient in the delivery system. The choice of the different formulations to be tested is carried out employing an axial design with constraint domains. The limits of each component were fixed on the basis of preliminary trials. The analysis of the $t_{50\%}$ values revealed that the release kinetics is mainly affected by stearic acid and theophylline content, whilst lactose effect is almost negligible. A substantial correspondence between the experimental results and the analysis of the drug release kinetics performed by means of an ad hoc developed mathematical model was found. The proposed mathematical model allows to conclude that wherever the release mechanism is initially ruled by dissolution, then diffusion plays the most important role.

Keywords: Melt extrusion; Ram extruder; Sustained release; Mathematical modelling; Theophylline

1. Introduction

Melt extrusion is the process of converting a raw material into a product of uniform shape and density by forcing it through die under controlled conditions. This process, extensively used in the plastic and rubber industry since the turn of the century, has found today its place in the pharmaceutical field [1]. For example, melt extrusion has been applied to the manufacturing of solid dispersions, granules, pellets, tablets, suppositories, implants, stents, transdermal systems and ophthalmic inserts. Depending on the pharmaceutical applications, various melt extruders are currently available in different designs. Typically, an extruder consists of two distinct parts: a conveying system which transports the material and in some

* Corresponding author. Tel.: +39-40-558-3435; fax: +39-40-569-823.
E-mail address: mariog@dicamp.univ.trieste.it (M. Grassi).

0168-3659/$ - see front matter © 2003 Elsevier B.V. All rights reserved.
doi:10.1016/S0168-3659(03)00330-4

cases imparts a degree of distributive mixing, and a die system which shapes as required. Depending on the shape of the die, the final product may take the form of a film, pipe, granule or, more simply, a cylinder. Thus, the potential of this technology exists of manufacturing a finished product directly by extrusion. Although in the pharmaceutical field, the most common apparatus are the screw extruders [2], recently the ram-extrusion technology has been successfully applied for the preparation of a cylindrically shaped fast-release formulation for carbamazepine, using polyethylene glycol 4000 as a low melting binder and lactose as a filler [3].

During the melt extrusion process in ram extruder, the mixture of binder, drug and excipients is introduced into the heated barrel, packed to a constant volume and extruded through the die attached at the end of the barrel. The molten polymer solidifies rapidly as the extrudate comes out the machine.

The goal of the present study was to evaluate the possibility of developing a cylindrical sustained-release dosage form by a ram extrusion process. For its large use in the pharmaceutical field monohydrated theophylline was chosen as a model drug. On the basis of previous successful melt pelletisation experiments [4,5], stearic acid was selected as a lipophilic low melting binder. Several formulations containing theophylline, stearic acid, polyethylene glycol 6000 and monohydrate lactose as hydrophilic fillers were prepared. The effect of the percentage and the type of components on release kinetics was evaluated with the help of an experimental design for mixtures while the study of the release mechanism was performed by means of a mathematical model.

2. Materials and methods

2.1. Materials

Theophylline E.P. grade (Faravelli, Milan, Italy), stearic acid reagent grade (Galeno, Milan, Italy), monohydrate lactose EP grade (Pharmatose 200 mesh, Meggle, Wasserburg, Germany) and polyethylene glycol 6000 (PEG) reagent grade (Veronelli, Milan, Italy) were used as starting materials.

The drug and lactose particle sizes are determined by microscopical analysis technique (Olympus BH-2 microscope, equipped with a computer-controlled image analysis system Optomax V, Cambridge, UK). The mean diameter (± S.D.) of theophylline is 56 (± 18) μm, while it is for lactose 16 (± 11.3) μm.

The melting range of stearic acid and PEG 6000 were estimated by a differential scanning calorimeter (Mod. TA 4000, equipped with a measuring cell DSC 20 Mettler, Greifensee, Switzerland). Samples of about 8 mg were placed in pierced aluminium pans (nominal capacity of 40 μl) and heated from 25 to 100°C at scanning rate of 10°C/min, under air atmosphere. Stearic acid and PEG melting temperature is 58.3 and 65.0°C, respectively.

2.2. Equipment

The extrudates were prepared using a laboratory scale ram extruder (Thalassia®, Trieste, Italy) sketched in Fig. 1. The movement of the stainless steel ram is promoted by an oleodinamic cylinder powered by an electric pump. The nickel-plated brass cylindrical barrel, has a capacity of 66 cm^3 and an inner diameter of 25 mm. Four different interchangeable cylindrical dies made of nickel plated brass can be attached at one end of the barrel, with a conical entry (120°), an inner diameter of 3, 2.5, 2, 1.5 mm and a length of 0.837 cm. The barrel is thermo-stated with

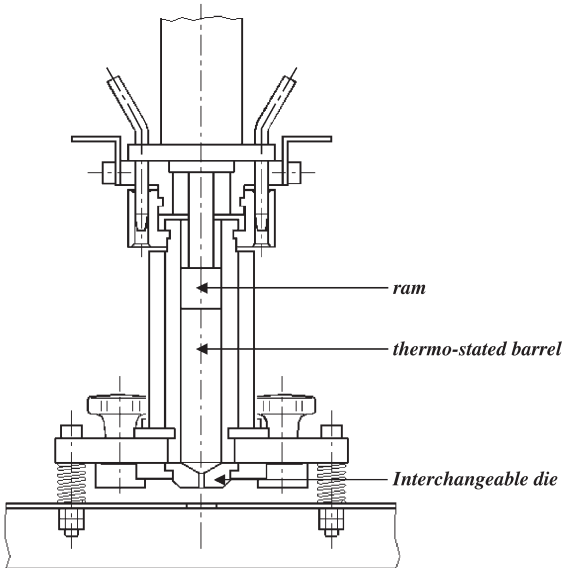

Fig. 1. Schematic drawing of the Thalassia® ram extruder.

an electrically heated jacket (maximum temperature about 120 °C). The maximal extrusion pressure is 15 MPa (150 bar).

2.3. Extrusion procedure

All components (300 g batch size) were first mixed in 2.8 dm^3 one-step mixer (Rotolab® Zanchetta, Lucca, Italy) for 10 min at 120 rpm in the appropriate relative proportions (according to the experimental plan reported in Table 1). Evaluation of the content homogeneity of the final extrudate proved the mixing process successful. Then, 30 g mixture were taken from the bulk and packed to a constant volume, by applying hand pressure, into the barrel, previously thermo-stated at the chosen temperature. In order to check the processability of various formulations depending on the temperature, preliminary experiments were carried out using different temperatures. On the basis of these preliminary trials, the temperature of 53 °C, allowing to successfully produce an extrudate with uniform shape and satisfactory smooth surface, was selected. After the equilibration time (20 min), the mass was extruded through the 3-mm diameter die, using a constant velocity for the piston. Once the samples had cooled to ambient temperature, the extrudates were sliced up in cylinders of approximately 5 mm length and 3 mm diameter using a hot cutter.

2.4. Experimental design

A particular experimental design was planned in order to study the effect of the concentration of each component in the presence of all the others, on the drug release rate with the least number of trials. In particular, the Cox axial design with constraint domain, typically used for mixture screening processes [6], was employed. The constraint domain for each component is fixed on the basis of the preliminary trials, the range of the percentage for each component being: 10–75% for monohydrate theophylline, 25–90% for stearic acid, 0–15% for monohydrate lactose and 0–15% for polyethylene glycol 6000. The quantitative constraints for each component define a polyhedral experimental domain located inside the original tetrahedron, with the pure components at the vertices. In the Cox axial design the experiments are distributed in the axes, included in the experimental polyhedron. These axes join every pure component (vertices of the tetrahedron) to the opposite face of the figure passing through the barycentre of the polyhedron

Table 1
Percent composition of the extrudates and measured response ($t_{50\%}$)

No.	Components				$t_{50\%}$ (h)
	$100*\omega_{THEO}$	$100*\omega_{SACID}$	$100*\omega_{LACT}$	$100*\omega_{PEG}$	
1	10.05	69.19	10.38	10.38	8.00
2	29.09	54.55	8.18	8.18	9.00
3	48.13	39.40	5.98	5.98	1.70
4	67.17	25.25	3.79	3.79	4.50
5	52.46	25.05	11.24	11.24	1.50
6	38.37	45.19	8.22	8.22	5.25
7	24.28	65.32	5.20	1.04	>24 (27.50[a])
8	10.18	85.45	2.18	2.18	>24 (70.00[a])
9	37.81	54.01	0.08	8.10	9.50
10	35.94	51.34	5.03	7.70	6.50
11	34.06	48.66	9.97	7.30	9.00
12	32.19	45.99	14.92	6.90	7.25
13	37.81	54.01	8.10	0.08	18.50
14	35.94	51.34	7.7	5.03	12.50
15	34.06	48.66	7.30	9.97	6.50
16	32.19	45.99	6.90	14.92	5.00
17	35.00	50.00	7.50	7.50	9.00

[a] The values are calculated by means of the proposed mathematical model.

(corresponding in this case to system 17) (see Table 1 and Fig. 3). The compositions of tested mixtures were calculated with the help of NEMRODW program [7]. Table 1 reports the composition of the 17 performed systems. Since the aim of this work was to obtain a sustained release dosage form for theophylline and to study the effect of each component on the drug release, the time required for 50% of drug dissolution ($t_{50\%}$) was used as measured response.

2.5. Characterisation of the extrudates

2.5.1. In vitro dissolution studies

The dissolution test was performed according to the USP 24 method I. A dissolution rotating basket apparatus SOTAX (AT 7 Smart, Basel, Switzerland) was employed with a stirring rate of 100 rpm and maintained at $37 \pm 0.1\,^{\circ}C$. Samples of extrudates of 5 mm length and of 3 mm diameter, containing a suitable amount of theophylline for sink conditions ($C \ll Cs$), were dissolved in 900 ml of dissolution medium (freshly demineralised water). The aqueous solution was filtered and continuously pumped to a flow cell in spectrophotometer Perkin-Elmer (mod. Lambda 35, Monza, Italy) and absorbance values were recorded at the maximum wavelength of the drug (271 nm). PEG, stearic acid and lactose did not interfere with the UV analysis. The results are the average of triplicate experiments, and standard deviation never exceeded 2% of the mean values.

2.5.2. Intrinsic dissolution rate studies

Intrinsic dissolution rate studies were performed in 150 ml of freshly demineralised water ($T = 37 \pm 0.1\,^{\circ}C$). Non disintegrating disks of 10 mm diameter were prepared by double compression of 150 mg of the crystalline material at a load of 3 tons in a manual tablet presser (Perkin-Elmer, Norwalk, USA). XRD confirmed that the crystal form of the original powder was retained following the compression procedure. The USP 24 dissolution apparatus (Mod. DT-1, Erweka, Heusenstamm, Germany), was used equipped by a beaker having a nominal capacity of 250 ml instead of the conventional vessel. The shaft, usually employed for holding the basket, served to hold the paraffin-mounted disk, thus allowing only one surface to be exposed to the dissolution medium. The theophylline disk was placed at 2.0 cm from the beaker bottom containing dissolution medium. In order to measure theophylline diffusion coefficient D_w in the dissolution environment according to Levich theory [8,9], different shaft angular velocities were considered: 60, 80, 100, 150 and 185 rpm. The aqueous solution was filtered and continuously pumped to a flow cell in a spectrophotometer and absorbances were recorded at 271 nm. Experimental points were the average of at least three replicates and standard deviations never exceeded 2% of mean value.

2.5.3. X-ray photoelectron spectroscopy (XPS)

XPS measurements were performed in a ultra high vacuum chamber working at a base pressure of about 1×10^{-7} mbar, equipped with a conventional Mg-anode X-ray source (Physical Electronics, Eden Prairie, US, Mod. 20095) ($h\upsilon = 1253.6$ eV) and a double pass Cylindrical Mirror Analyzer (PHI Physical Electronics, Eden Prairie, US, Mod. 15–255 g). The samples were prepared by pressing a suitable amount of pellets onto foils of pure tantalum (99.999% purity, Goodfellow, Huntingdon, UK).

The *C*1s, *N*1s and *O*1s concentrations (conc.) were calculated from the areas of the XPS measured spectra, taking into account the sensitivity factors (*s*) of the elements onto the surface, with the help of the following equation (e.g., for *N*1s):

$$\text{conc.}(N1s) = \frac{\text{area}(N1s)/s(N1s)}{\text{area}(N1s)/s(N1s) + \text{area}(C1s)s(C1s) + \text{area}(O1s)/s(O1s)} \quad (1)$$

2.5.4. True density measurement

True density was measured with helium pycnometer (Multi-pycnometer, Quantachrome, Boynton Beach, USA) in a 35-cm^3 cell calibrated with a steel sphere. The measurements were taken in triplicate experiments.

3. Modelling of drug-release mechanism

Drug release from this kind of delivery systems is a complex phenomenon substantially ruled by drug dissolution and diffusion through the fluid filling the channels pervading the insoluble matrix [10]. The complexity of the topology of the matrix (e.g., chang-

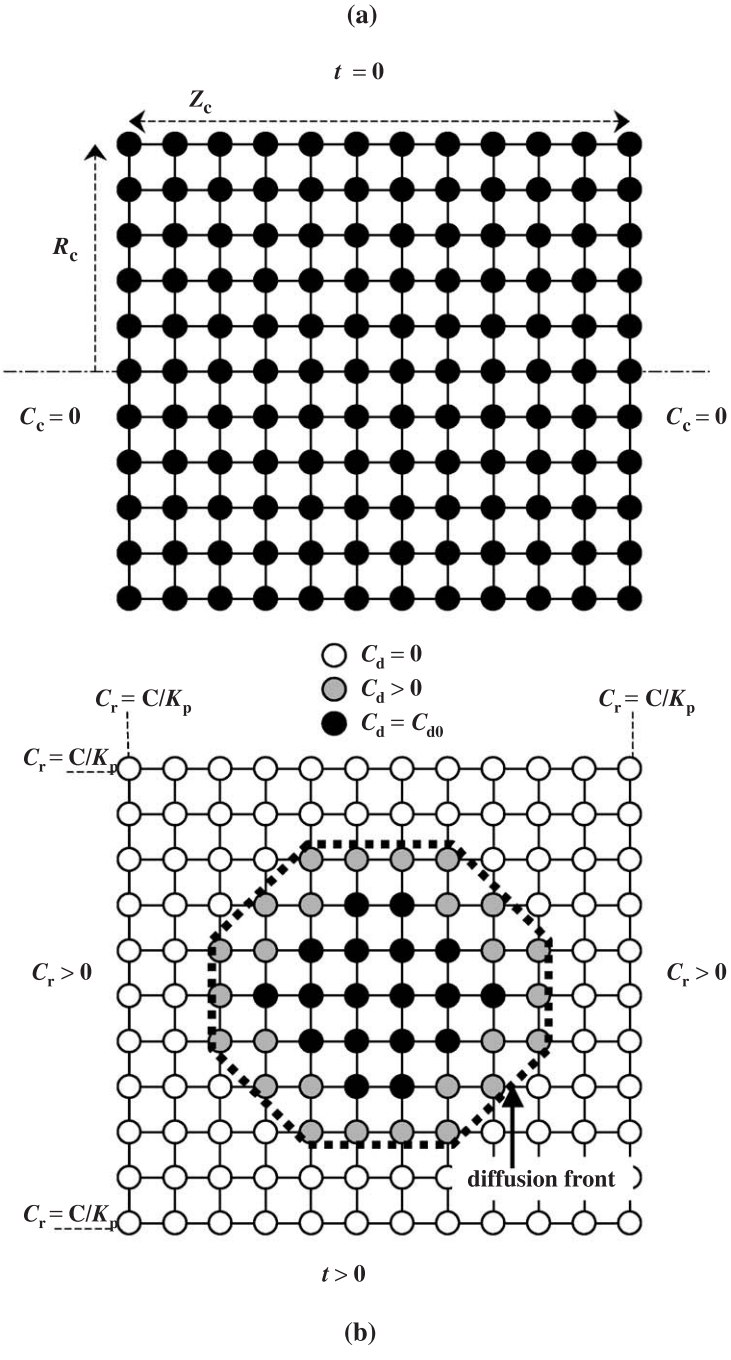

Fig. 2. Schematic representation of the cylindrical delivery system at the beginning of the release experiments (a) and for $t>0$ (b). Filled circles indicate that not dissolved drug concentration C_d is bigger than 0, while open circles indicate that $C_d=0$ (vertical and horizontal bars indicate the computational grid). Anytime, the amount of drug present in the delivery system and in the release environment must be constant (Eq. (9)).

ing porosity) due to the dissolution of theophylline, PEG and lactose, makes any attempt of a detailed matrix description in terms of Euclidean geometry meaningless. A fractal approach could be useful to this purpose, but it would result in a considerable complication when writing the equation ruling mass transfer [11].

Although the matrix is an inhomogeneous system (the drug molecules diffuse only inside the fluid filling the channels and no drug transport occurs through the insoluble channel walls), matrix homogeneity is assumed. This entails the definition of an effective drug diffusion coefficient D_e characterising drug molecules motion in the cylindrical matrix [12]. Moreover, it can be considered that soluble compounds (PEG, lactose) instantly dissolves upon contact with environmental fluid and that the topology of matrix channels is not affected by drug dissolution. For the model to be closer to reality, it is supposed that two different values of the effective drug diffusion coefficient D_e can be distinguished: D_{ee} (higher) related to the matrix surface and the just-underneath-the surface thin layer (thickness h), D_{ei} (lower) related to the inner part of the matrix. Indeed, while it is more than reasonable that the outer matrix layer should be instantly pervaded by external fluid, the inner part, due to matrix topology, is wetted only later. Accordingly, instantaneous dissolution of soluble compounds (PEG, Lactose) takes place only in the outer matrix layer. As a consequence, average matrix porosity in the inner part is lower than that in the outer part, therefore two distinct effective diffusion coefficients are necessary to describe this situation.

Additionally, it is supposed that matrix density does not vary as a function of the diffusion and that cylindrically shaped matrices with perfectly cylindrical shape undergo neither erosion nor swelling during the release process. At the beginning, the cylindrical matrices are surrounded by a stagnant layer, whose thickness depends on the hydrodynamic conditions imposed on the release environment. The layer hinders drug diffusion into the dissolution medium, it is assumed that this resistance is negligible in comparison with drug dissolution and diffusion inside the insoluble matrix.

On the basis of these hypotheses, and on the assumption that no mass diffusion takes place in the angular direction due to matrix cylindrical symmetry, the whole drug release process can be schematically represented by the following two-dimensions (radial and axial) equation:

$$\frac{\partial C}{\partial t} = \frac{1}{R}\frac{\partial}{\partial R}\left[RD_e\frac{\partial C}{\partial R}\right] + \frac{\partial}{\partial Z}\left[D_e\frac{\partial C}{\partial Z}\right] - \frac{\partial C_d}{\partial t} \tag{2}$$

$$\frac{\partial C_d}{\partial t} = -K_t(C_s - C) \tag{3}$$

where t is time, R and Z are, respectively, radial and axial co-ordinate, C and C_d are, respectively, the concentrations of the dissolved and not dissolved drug fractions, K_t is the dissolution constant and C_s is the drug solubility in the release fluid. Eq. (2) illustrates the differential drug mass balance, while Eq. (3) illustrates the drug dissolution process occurring upon drug contact with the release fluid [13–18].

Eq. (2) is numerically solved (control volume method [19]) with the following initial conditions (see Fig. 2):

$$C_r = 0 \tag{4}$$

$$C(R,Z) = 0 \quad 0 < R < R_c \quad 0 < Z < Z_c \tag{5}$$

$$C_d(R,Z) = C_{d0} \quad 0 < R < R_c \quad 0 < Z < Z_c \tag{6}$$

and boundary conditions:

$$\frac{\partial C}{\partial R}\Big|_{R=0} = 0 \quad 0 < Z < Z_c \tag{7}$$

$$C_r = \frac{C}{K_p} \quad \text{cylinder surface} \tag{8}$$

$$M_0 = V_r C_r + N\int_0^{Z_c}\int_0^{R_c}[C(R,Z) + C_d(R,Z)]2\pi R\,dR\,dZ \tag{9}$$

where N is the number of considered cylindrical matrices, R_c and Z_c are, cylinder radius and height, respectively, C_{d0} is the initial not dissolved drug concentration, C_r is the drug concentration in the release environment, K_p is the drug partition coefficient, M_0 is the initial drug amount and V_R is the volume of the release environment. Eqs. (4)–(7) set ordinary and clear conditions, while Eq. (8) ensures

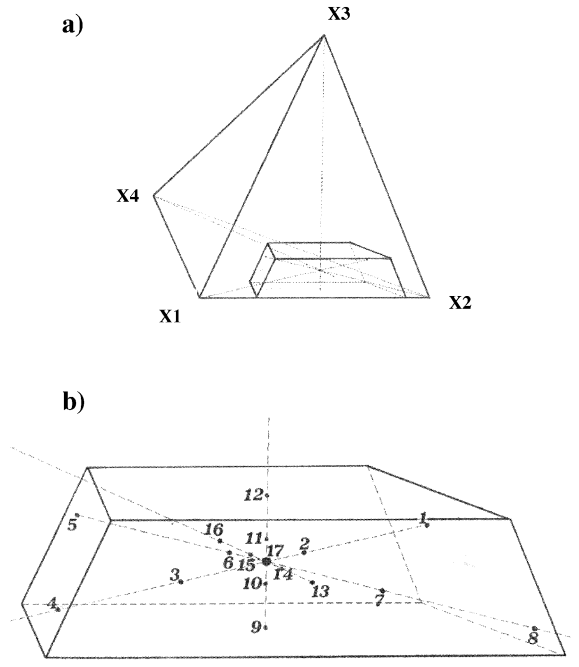

Fig. 3. The four-component constrained region defined by the (a) constraints $0.10 = \times 1\ (=\omega_{THEO}) = 0.75$; $0.25 = \times 2\ (=\omega_{SACID}) = 0.90$; $0 = \times 3\ (=\omega_{LACT}) = 0.15$, $0 = \times 4\ (=\omega_{PEG}) = 0.15$, and (b) Cox axial design.

the partitioning condition at the matrix/dissolution medium interface. Eq. (9) gives the total drug mass balance given by the sum of the drug in the release environment and the drug still present in the matrix. Eq. (9) substitutes the more common flux condition at the matrix/release environment interface [20], thus ensuring a more reliable and safe numerical solution for the model [21].

In order to get a reasonable compromise between numerical accuracy and time required to perform the numerical solution, the computational time step Δt is set at 60 s and a two-dimensional grid of 20×20 (for a total of 400 control volume elements) is considered.

4. Results and discussion

4.1. Preliminary considerations

Since drug release kinetics is highly influenced by the external cylinder area it is interesting to make some considerations about the shape of the cylindrical matrices before analysing the experimental data. Since the shape factor k is defined as the ratio between cylinder height Z_c and cylinder radius R_c, the external cylinder area A_c is given by:

$$A_c = 2\pi R_c^2(1+k) \tag{10}$$

Assuming the cylindrical volume V_c constant, the dependence of A_c on k is as follows:

$$R_c = \sqrt[3]{\frac{V_c}{\pi k}} \quad A_c = 2\sqrt[3]{\pi V_c^2}\frac{1+k}{k^{2/3}} \tag{11}$$

Recalling the expression of the A_c derivative with respect to k:

$$\frac{dA_c}{dk} = \frac{2\sqrt[3]{\pi V_c^2}}{3}\left(\frac{k-2}{k^{5/3}}\right) \tag{12}$$

it is easy to verify that $A_c(k)$ decreases in the range $0<k<2$, increases for $k>2$ showing a minimum for $k=2$. Moreover, it easy to numerically verify (for $V_c \le 0.1$ cm^3) that in the range $1.5<k<3.5$, $A_c(k)$ has an almost flat profile whose value nearly coincides with its minimum $A_c(k=2)$. Accordingly, in order to get the smallest external surface and thus the lowest release kinetics (regardless of the cylinder volume), the shape factor has to lie in the range $1.5<k<3.5$. For the above reasons and in the light of our cylinder production system, $k=3.3$ was chosen in this work.

The 17 systems are characterised by macroscopic and microscopic variables. In particular, $t_{50\%}$ is a macroscopic variable independent from any theoretical interpretation of the release mechanism, while effective drug diffusion coefficient (D_e) and drug dissolution constant (K_t) are microscopic variables based on a theoretical frame. $t_{50\%}$ has the obvious advantage of an ease determination despite not providing any information about its variations as instead provided by microscopic parameters D_{ei}, D_{ee} and K_t. Therefore, these two different approaches for data analysis were compared.

4.2. Macroscopic characterisation

The 17 systems were run randomly and the relative $t_{50\%}$ values are reported both in Table 1 and Fig. 4. The abscissa of the figure is ω, the

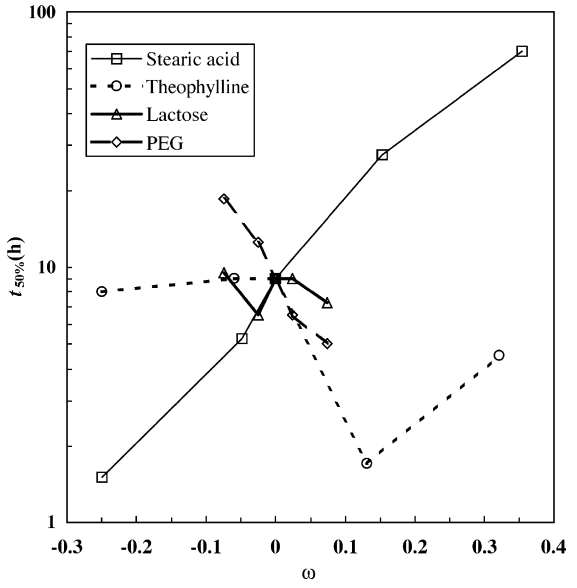

Fig. 4. Dependence of $t_{50\%}$ on ω for the systems studied (stearic acid, open squares tests 5–8; theophylline, open circles 1–4; lactose, open triangles tests 9–12; PEG, open rhombi tests 13–16).

difference between the composition of the reference mixture (sample 17) and each test mixtures. As it can be noticed, Fig. 4 highlights that the most significant effect on the $t_{50\%}$ is ascribable, as expected, to stearic acid. Indeed, it is reasonable that the increase of stearic acid mass fraction ω_{SACID} reduces matrix porosity, thus increasing its hindering action on drug release. Lactose mass fraction ω_{LACT} variation does not reflect in a sensible $t_{50\%}$ modification, while the effect of PEG mass fraction ω_{PEG} variation is more pronounced causing the reduction of $t_{50\%}$ from 18.5 h (system 13, low PEG content) to 5 h (system 16, high PEG content). Accordingly, it could be argued that the increase of ω_{PEG} could give rise to a more branched channel network in the matrix that favours drug release. Finally, a reduction of $t_{50\%}$ can be observed (Fig. 4 and Table 1) when theophylline mass fraction ω_{THEO} increases especially when ω_{THEO} exceeds that of system 17 (ω>0). It can be concluded that, generally speaking, an enrichment of water soluble compounds in the matrix produces an increase of matrix porosity, thus promoting a faster drug release.

4.3. Microscopic characterisation

4.3.1. System 17

As a second approach for the analysis of the data, the above-mentioned mathematical model based on the microscopic variables was used. Before performing data analysis, however, some considerations on data fitting procedure is necessary. Although D_{ee}, D_{ei}, K_t and h are real model fitting parameters, in order to greatly reduce the computational time required for data fitting (our model requires a numerical solution) the following strategy was adopted in setting h and K_t values. On the basis of numerical simulations led assuming test 17 conditions, it was found that the predicted release curve remarkably changes when at least 9% of the total drug contained in the cylinder belongs to the higher drug diffusion coefficient (D_{ee}) zone. It is easy to demonstrate that this corresponds to $h = 58$ μm. Similarly, $h = 115$ μm corresponds to 18% of the total drug belonging to the higher drug diffusion coefficient (D_{ee}) zone. Moreover, we found that when K_t exceeds 0.1 cm/s, the rate determining step is not dissolution but diffusion, and further K_t increases do not reflect in substantial drug release curve modifications. On the contrary, when $K_t < 0.1$ cm/s, obviously, data fitting yields higher D_{ei} and D_{ee} values but data description is not completely satisfactory (we get a higher sum of the squared differences between experimental data and model best fitting). Accordingly, data fitting is performed fixing discrete h values (0, 58, 115 μm and so on), setting $K_t = 0.1$ cm/s and letting D_{ei} and D_{ee} free to be modified.

Fig. 5 shows a good agreement between model best fitting (solid thick line) and experimental data (black circles) relative to system 17 (pivot system). So as to take the comparison more significant, test 17 is added as a reference and the dimensionless quantity C_r^+, indicating the ratio between C_r and its value after a very long time ($C_{r\infty}$), is considered. For the sake of clarity, data standard errors ranging among 0.2–2.0% have been omitted for all the in vitro dissolution profiles. This fitting-performed in the knowledge that release volume $V_r = 900$ cm^3, cylinder height $Z_c = 0.5$ cm, cylinder radius $R_c = 0.15$ cm ($k = 3.33$), $M_0 = 26.4$ mg (this corresponds to $N = 2$ cylinders), fixing $K_t = 0.1$ cm/s- yields $D_{ee} =$

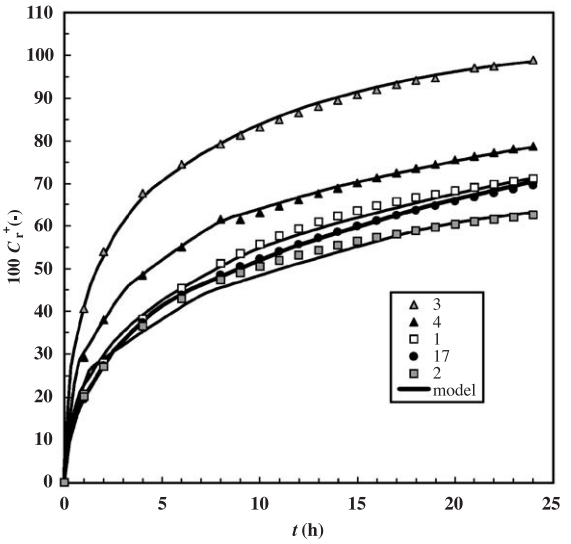

Fig. 5. Temporary trend of the dimensionless theophylline concentration C_r^+ in the receiver environment (test 3, grey triangles; test 4, black triangles; test 1 open squares; test 17 black circles; test 2 grey squares; solid line model best fitting. For the sake of clarity, datum standard error, ranging among 0.2–2.0%, has been omitted).

2×10^{-6} cm^2/s, $D_{ei} = 4.2 \times 10^{-7}$ cm^2/s where D_{ee} and D_{ei} are, respectively, the effective diffusion coefficient in the outer matrix layer (thickness $h = 58$ μm) and in the inner part (see also Table 2). This figure supports the reasonability of the physical hypotheses on which the model has been built, and, particularly, the assumption of a homogeneous matrix characterised by an effective diffusion coefficient. It is further interesting noticing that, despite the small h value, data fitting would not be satisfactory had the existence of the external layer of thickness h (characterized by a much higher diffusion coefficient) been neglected. In particular, the model would not be able to properly fit both the initial (0–4 h) and the final part of the release curve since it could not describe simultaneously the initial burst effect (typical of tablets [22]) and the following part characterised by a slower release kinetics. This particular kind of release kinetics can be explained because in the outer part of the matrix, drug release is mainly ruled by drug dissolution and drug diffusion plays a less important effect, due to the thin diffusion layer. In the inner part, in contrast, drug diffusion is the limiting step. As a consequence, drug release is considerably slowed down. The presence of theophylline on the cylinder surface is confirmed by an XPS analysis. Indeed, the nitrogen peak detected analysing the pure theophylline at about 405 eV [4], and still present in the spectrum of the extrudates, demonstrated the presence of the drug on the surface of the cylinders. In particular, the drug

Table 2
Theophylline amount (M_0), fitting parameters (K_t, D_{ei}, D_{ee}, h), tortuosity (τ_i, τ_e), initial (ε_1) and final (ε_2) porosity of the 17 systems studied

No,	M_0 (mg)	K_t (cm/s)	D_{ei} (cm^2/s)	D_{ee} (cm^2/s)	h (μm)	τ_e (−)	τ_i (−)	ε_1 (−)	ε_2 (−)
1	24.6	0.1	3.40×10^{-8}	1.40×10^{-7}	115	293.6	1208.9	0.164	0.239
2	23.0	0.1	1.25×10^{-7}	1.10×10^{-6}	115	36.5	321.8	0.136	0.367
3	24.8	0.1	1.90×10^{-6}	1.00×10^{-5}	115	4.6	24.0	0.105	0.510
4	26.5	0.1	1.80×10^{-7}	7.00×10^{-6}	115	8.9	77.8	0.071	0.670
5	22.1	0.1	6.00×10^{-6}	1.00×10^{-5}	115	2.5	4.2	0.210	0.675
6	16.8	0.1	9.00×10^{-7}	2.50×10^{-6}	58	14.8	41.0	0.142	0.457
7	19.0	0.1	8.50×10^{-8}	6.50×10^{-7}	58	96.4	737.8	0.083	0.270
8	23.8	0.1	8.00×10^{-9}	5.00×10^{-8}	115	3197.8	19986.2	0.033	0.105
9	27.7	0.1	4.00×10^{-7}	2.00×10^{-6}	58	32.2	161.0	0.074	0.374
10	27.0	0.1	5.30×10^{-7}	1.25×10^{-6}	115	37.3	87.9	0.109	0.397
11	26.6	0.1	1.75×10^{-7}	1.50×10^{-6}	115	24.7	211.5	0.145	0.422
12	25.1	0.1	2.80×10^{-7}	1.60×10^{-6}	115	19.3	110.4	0.062	0.365
13	27.0	0.1	2.00×10^{-7}	2.20×10^{-6}	58	34.0	374.3	0.182	0.446
14	27.3	0.1	3.10×10^{-7}	1.60×10^{-6}	58	30.0	154.8	0.105	0.395
15	25.7	0.1	4.00×10^{-7}	1.50×10^{-6}	115	24.2	90.7	0.149	0.424
16	23.5	0.1	3.60×10^{-7}	2.00×10^{-6}	115	14.8	82.1	0.192	0.454
17	26.4	0.1	4.20×10^{-7}	2.00×10^{-6}	58	20.6	98.1	0.127	0.410

concentration on the surface of the systems, calculated by means of the Eq. (1), was 5.75%.

On the basis of the calculated effective diffusion coefficient (D_{ei}, D_{ee}) and knowing that the theophylline diffusion coefficient D_w in the dissolution medium ($T=37\,^{\circ}C$) is equal to 8.0×10^{-6} cm^2/s (determined with the method reported in the section of 'intrinsic dissolution rates studies'), the tortuosity τ of the matrices can computed according to the well known equation [12]:

$$\tau = \frac{D_w}{D_e^* \varepsilon} \tag{13}$$

where ε is the matrix void fraction. The ε value varies with time because the hydrophilic excipients (lactose, PEG) and theophylline dissolve. Consequently, it was decided to calculate τ assuming two distinct ε values and then averaging the resulting τ values. Accordingly, ε is estimated at the beginning of the release process (theophylline is not dissolved and excipients are considered totally dissolved; $\varepsilon_1=0.13$) and at the end, when the matrix consists of stearic acid alone ($\varepsilon_2=0.41$). Hence $\tau_e=20.6$ and $\tau_i=98.1$ are found, where τ_e and τ_i are, respectively, the matrix tortuosity in the outer layer and in the inner part (see also Table 2).

4.3.2. Other systems

Fig. 5 also shows the comparison between model best fitting (solid line) and the experimental data (symbols) relative to tests 1, 2, 3 and 4. While the model is clearly able to fit properly the experimental data regardless of the test, the effect of theophylline concentration (ω_{TEO}) on release kinetics is remarkable since increasing concentration speed up drug release (tests 3 and 4) compared to test 17. This can be explained considering that the higher the theophylline content, the lower the hindering effect exerted by the stearic acid matrix due to a bigger initial (ε_1) and final (ε_2) matrix void fraction. Indeed, as soon as drug dissolves, matrix porosity rapidly increases even more so as drug content increases and this process becomes more and more important for higher drug content (see Table 2 for different porosities relative to system 1–4). The lower kinetics release of test 4 compared to test 3 could be ascribed to a diffusion hindering phenomenon due to a crowding effect [12] of drug molecules inside the water-filled matrix channels as shown in Fig. 6. This figure reports the internal and external effective diffusion coefficient trend (D_{ei}, D_{ee}, respectively) (coming from data fitting), for the 17 studied tests as a function of ω, the difference between a reference composition (respectively, test 17 ω_{TEO}, ω_{SACID}, ω_{LAT} and ω_{PEG} for tests 1–4, 5–8, 9–12 and 13–16) and the current test composition (respectively, ω_{TEO}, ω_{SACID}, ω_{LAT} and ω_{PEG} for tests 1–4, 5–8, 9–12 and 13–16). It can be observed that whereas D_{ei} and D_{ee} increase from test 1 to test 3, they decrease for test 4. It is interesting noticing that also for tests 1–4 in order to have a good data fitting the model requires the existence of an external matrix layer (whose thickness is reported in Table 2) characterised by a higher diffusion coefficient (K_t is always equal to 0.1 cm/s).

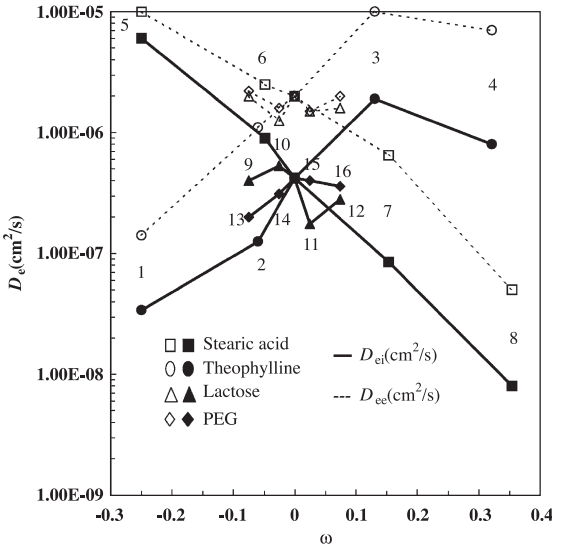

Fig. 6. Dependence of the external D_{ee} (black symbols, solid line) and the internal D_{ei} (open symbols, dashed line) effective diffusion coefficient on ω for the systems studied (stearic acid, squares tests 5–8; theophylline, circles 1–4; lactose, triangles tests 9–12; PEG, rhombi tests 13–16).

Fig. 7 illustrates the comparison between model best fitting (solid line) and experimental data (symbols) referring to tests 5–8. While for tests 5 and 6 data description is very good, the description of the initial stages of tests 7 and 8 is not. This is probably

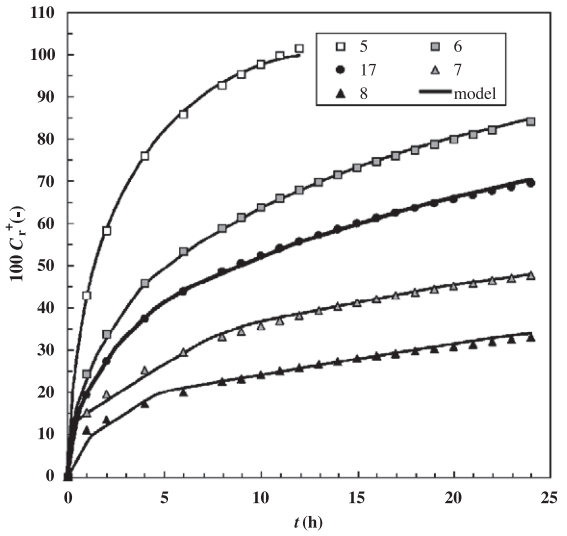

Fig. 7. Temporary trend of the dimensionless theophylline concentration C_r^+ in the receiver environment (test 5, open squares; test 6, grey squares; test 17 black circles; test 7 grey triangles; test 8 black triangles; solid line model best fitting. For the sake of clarity, datum standard error, ranging among 0.2–2.0%, has been omitted).

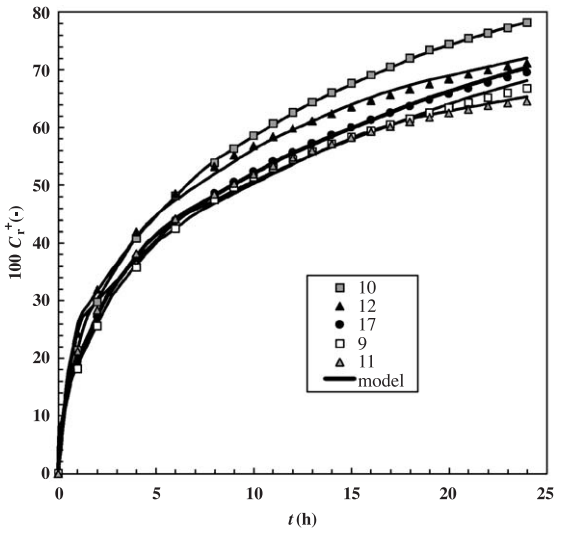

Fig. 8. Temporary trend of the dimensionless theophylline concentration C_r^+ in the receiver environment (test 10, grey squares; test 12, black triangles; test 17 black circles; test 9 open squares; test 11 grey triangles; solid line model best fitting. For the sake of clarity, datum standard error, ranging among 0.2–2.0%, has been omitted).

because model assumption of an immediate dissolution of hydrophilic excipients (PEG and lactose) in the outer matrix part is not completely accurate due to the high hindering effect caused by the abundant insoluble matrix component (stearic acid). In any event, Fig. 7 clearly shows that the increase of the stearic acid mass fraction ω_{SACID} is responsible for a considerable reduction of both D_{ei} and D_{ee} determined by data fitting (as demonstrated in Fig. 6 and Table 2). This can be explained with the increase of ω_{SACID}, the matrix porosity proportionally diminishes and the matrix topology (here represented by external and internal tortuosity τ_e and τ_i) becomes more and more complex. Indeed, as shown in Table 2, τ_e and τ_i range, respectively, from 2.5 and 4.2 (test 5) to 3197 and 19986 (test 8). These considerations lead to the conclusion that ω_{SACID} is the most important variable for the modification of drug release kinetics in these kind of matrices, apart from cylinder shape factor k, as above discussed. Also for tests 5–8 data fitting requires an external matrix layer (see Table 2 for thickness) characterised by a higher drug diffusion coefficient (K_t is always equal to 0.1 cm/s).

Fig. 8 reveals that model best fitting (solid line) describes experimental data (symbols) referring to tests 9, 10, 11 and 12. Fitting procedure demonstrates that for a good data description, the existence of an external matrix layer characterised by a higher drug diffusion coefficient is required (see Table 2 for thickness entity), (K_t is always equal to 0.1 cm/s). In particular, Fig. 6 shows that both D_{ei} and D_{ee} (determined by data fitting) are not substantially affected by the variation of lactose mass fraction ω_{LACT}, indicating that ω_{LACT} is not critical for release kinetics control. Nevertheless, the fact that the release curves kinetics (see Fig. 8 and Table 2) and the D_{ei}, D_{ee} values (see Fig. 6) are not inversely proportional to stearic acid mass fraction ω_{SACID} suggests that lactose concentration can slightly modify matrix topology. This is probably the reason why, for example, $D_{ei} = D_{ee}$ for test 10 (stearic acid mass fraction $\omega_{SACID} = 0.5134$) are higher than those of test 11 (stearic acid mass fraction $\omega_{SACID} = 0.4866$) and test 12 (stearic acid mass fraction $\omega_{SACID} = 0.4599$).

Finally, Fig. 9 shows the comparison between model best fitting (solid line) and experimental data (symbols) referring to tests 13, 14, 15 and 16. Again, data

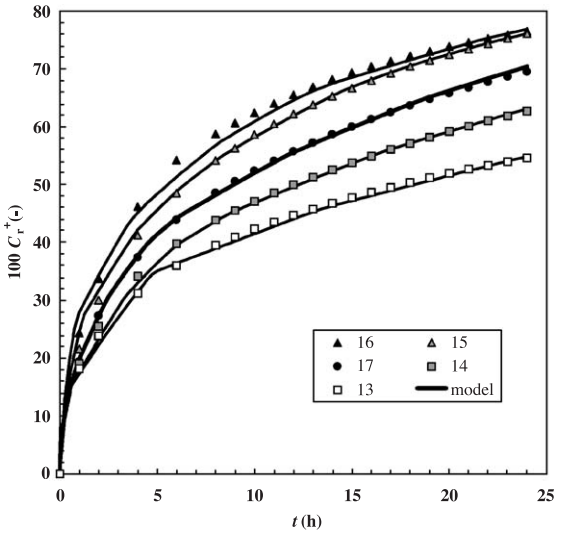

Fig. 9. Temporary trend of the dimensionless theophylline concentration C_r^+ in the receiver environment (test 16, black triangles; test 15, grey triangles; test 17 black circles; test 14 grey squares; test 13 open squares; solid line model best fitting. For the sake of clarity, datum standard error, ranging among 0.2–2.0%, has been omitted).

description is reasonably good for all tests by supposing the existence of an outer matrix layer characterised by a higher diffusion coefficient (see Table 2 for layer thickness), with $K_t = 0.1$ cm/s. While D_{ee} is mainly independent from PEG mass fraction ω_{PEG} (see Fig. 6), D_{ei} is directly proportional to ω_{PEG} even if for tests 15 and 16 it assumes similar values. This behaviour can be explained observing (see Table 2) that the thickness h of the outer matrix layer is higher than that of tests 13 and 14. Accordingly, it could be argued that the effect of PEG is to slightly increase matrix porosity and to improve the extent h of the matrix outer part characterized by an higher diffusion coefficient.

The comparison between the theoretical analysis and the one previously performed by means of $t_{50\%}$ shows how they point to the same conclusions. Nevertheless, the theoretical analysis can provide a more detailed picture of matrix topology which could be supposed using the simpler $t_{50\%}$ approach.

4.4. Model simulations

It is now interesting to analyse model simulations taking test 17 parameters as reference and varying shape factor k that, as discussed above, plays a very important role in drug release kinetics since it regulates cylinder external area. Much to this purpose, Fig. 10 reports the release curves ($0 < t < 24$ h) calculated according to our model with k ranges from 0.1 to 30. This interval includes typical values for cylindrical delivery systems. Clearly, whereas the lowest release kinetics takes place at the minimum cylinder external area ($k = 2$), release kinetics sharply increases for greater or lower k values. In order to confirm these model predictions, one additional experimental test was performed referring to test 17 conditions. While in test 17 $Z_c = 0.5$ cm and $R_c = 0.15$ cm ($k = 3.3$) are assumed as geometrical cylinder characteristics, the additional test is performed assuming $Z_c = 2$ cm and $R_c = 0.15$ cm ($k = 26.6$) (see Fig. 10). Certainly, these conditions guarantee that always the same amount of theophylline is added to the release environment. Although the experimental $t_{50\%}$ is about 6 h whilst the model prediction yields a $t_{50\%} \approx 4$ h, we can affirm that model prediction is qualitatively correct (we remember that test 17 $t_{50\%} \approx 9$). In other words, the bigger cylinder surface, the faster release kinetics. The

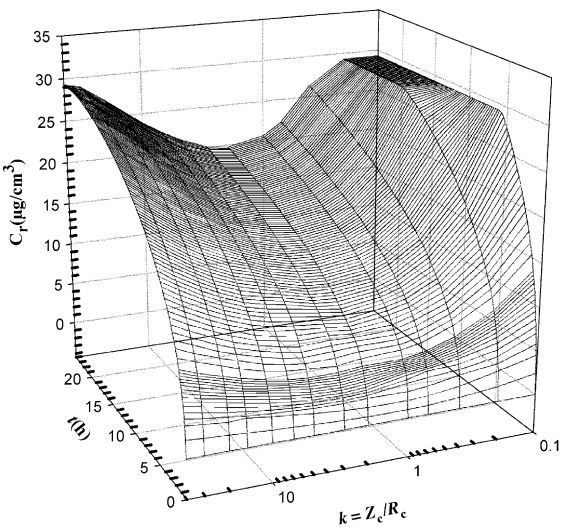

Fig. 10. Model prediction about the time evolution of the receiver drug concentration C_r considering different k ratios and assuming all other parameters equal to those of test 17. For $k = 2$ we can notice the slowest drug release kinetics.

lower experimental response in comparison to model prediction can be ascribed to the more compact structure of the extrudates resulting from the higher pressure needed to produce cylinders with a lower die diameter.

Finally, the position of the diffusion front [23–25] as time goes on for test 17 was plotted (Fig. 11) by using the model. This front subdivides the matrix region where not dissolved drug still exists (C_d>0) (inside front contour) from that (outside front contour) where drug is present only in the dissolved form (C_d=0 and C>0). Front position determination is straightforward as the software we built on to solve our model yields the determination of $C_d(R, Z, t)$ and $C(R, Z, t)$, being R, Z and t spatial co-ordinates and time, respectively. Accordingly, front position (whose resolution depends on the grid mesh used for the numerical solution) is chosen so that grid points inside the matrix region delimited by its contour are characterised by C_d>0, while outer points are characterised by C_d=0.

Fig. 11, showing the cylindrical matrix cross-section (abscissa, radial direction R; ordinate, axial direction Z), highlights, with solid lines, the position of the receding diffusion front at different times (1 min, 1 h, 32 h, 64 h and 96 h). Moreover, the dotted line (right ordinate axis), indicating the radial diffusion front velocity V_{df} (the same considerations can be made considering the axial directions) as a function of radial position (which, in turn, is a function of time), shows that V_{df} sharply decreases in the first 8 h and then becomes approximately constant after 32 h (the experiment lasted 24 h).

We would like to conclude this section observing that model potentiality could be implemented by simply considering a drug diffusion coefficient depending on matrix local porosity ε (which in turn, depends on time and position): $D=D(\varepsilon(R, Z, t))$. In this manner, indeed, the model will be able to indirectly provide useful information on the temporal

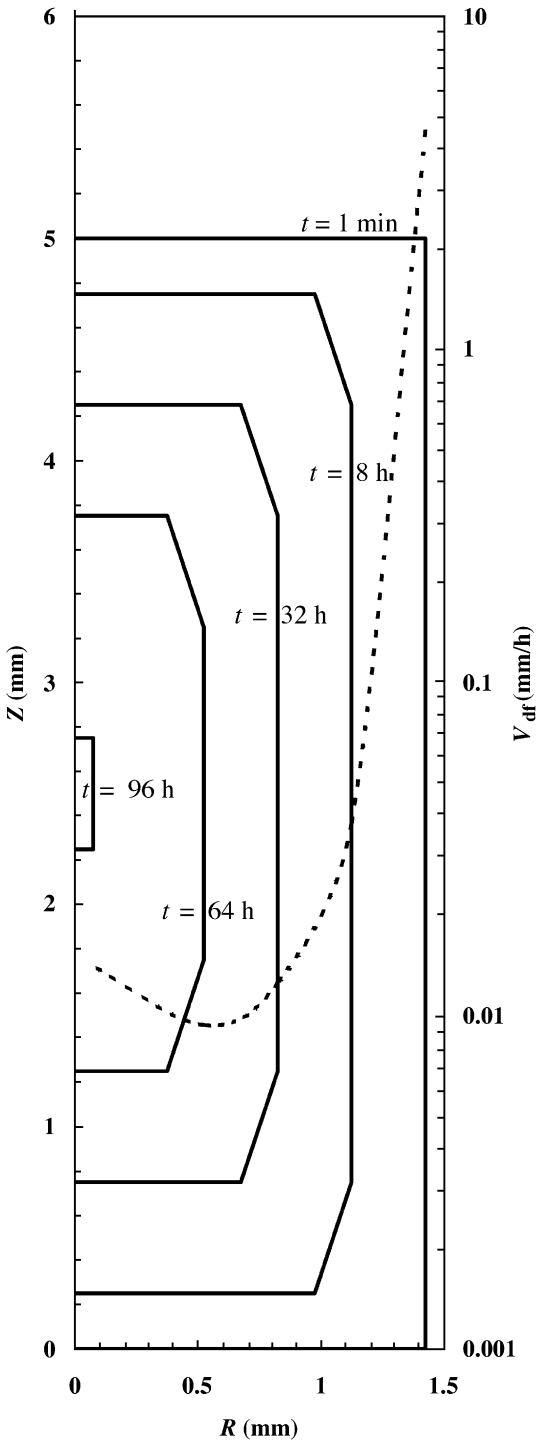

Fig. 11. Model prediction of the temporary evolution of the diffusion front position (solid line) inside the cylindrical matrix (Z, R axial and radial co-ordinate, respectively) assuming test 17 parameters. Dotted line indicates the diffusion front receding speed (V_{df}) in the radial direction.

evolution of matrix porosity due to drug and soluble compounds dissolution.

5. Conclusions

This work demonstrates that it is possible developing a cylindrical sustained-release dosage form for theophylline directly by means of a ram extrusion process. Obviously, a reliable designing requires a correct evaluation of the geometrical and compositional characteristics of the dosage form. Indeed, for a constant dose, the slowest release kinetics is achieved from a cylinder characterised by a height/radius ratio close to 2, as this condition corresponds to the smallest external cylinder area. Moreover, an analysis of experimental data performed according to the evaluation of $t_{50\%}$ (time required to release the 50% of the dose) evidences that release kinetics is essentially slowed down by the increase of stearic acid in the matrix. On the contrary, while the increase of theophylline and PEG determines an improvement of the release kinetics, lactose does not seem to affect remarkably the release process. Interestingly, the above conclusions substantially correspond with the results inferred from the ad hoc developed mathematical model. Obviously, this theoretical approach yields some other, more detailed, information about the release process. Indeed, a satisfactory data fitting requires to postulate the existence of an outer matrix layer characterised by an higher drug diffusion coefficient. Thus, at the early stage of the experiment, release kinetics is mainly ruled by drug dissolution and not by drug diffusion. On the contrary, subsequently, drug diffusion becomes the rate determining step of the entire release process. Finally, it can be concluded that the developed model is a reliable tool in the optimisation process of delivery system like those investigated in this work.

6. Nomenclature

A	theophylline powder surface area per unit mass
A_c	external cylinder area
C	concentrations of dissolved drug fraction
C_d	concentration of not dissolved drug fraction
C_{d0}	initial not dissolved drug concentration
C_r	drug concentration in the release environment
C_s	drug solubility in the release fluid
C_r^+	dimensionless quantity calculated as the ratio $C_r/C_{r\infty}$
$C_{r\infty}$	drug concentration in the release environment after a very long time
D_e	effective drug diffusion coefficient
D_{ee}	effective diffusion coefficient in the outer matrix layer
D_{ei}	effective diffusion coefficient in the inner part
D_w	theophylline diffusion coefficient in water ($T=37°C$)
K	shape factor (ratio between Z_c and R_c)
K_p	drug partition coefficient
K_t	dissolution constant
h	thickness of outer matrix layer
M_0	drug amount initially present in all the cylinder considered for dissolution
N	number of cylindrical matrices considered to resolve mass balance
R	radial co-ordinate
R_c	cylinder radius
t	time
$t_{50\%}$	time required for 50% of drug dissolution
V_r	volume of the release environment
V_{df}	radial diffusion front velocity
Z	axial co-ordinate
Z_c	cylinder height

7. Greek letters

ε	matrix void fraction
ε_1	matrix void fraction at the beginning of the release process
ε_2	matrix void fraction at the end of the release
τ	matrix tortuosity
τ_e	matrix tortuosity in the outer layer
τ_i	matrix tortuosity in the inner part
ω	difference between a reference composition (system 17) and current test composition for each component
ω_{THEO}	mass fraction of theophylline
ω_{SACID}	mass fraction of stearic acid
ω_{LACT}	mass fraction of monohydrate lactose
ω_{PEG}	mass fraction of poly-ethylene glycol 6000

References

[1] A. Forster, T. Rades, J. Hempestall, Selection of suitable drug and excipient candidates to prepare glass solutions by melt extrusion for immediate release oral formulations, Pharm. Tech. Eur. 14 (10) (2002) 27–37.

[2] J. Breitenbach, Melt extrusion: from process to drug delivery technology, Eur. J. Pharm. Biopharm. 54 (2) (2002) 107–117.

[3] B. perissutti, J.M. Newton, F. Podczeck, F. Rubessa, Preparation of extruded carbamazepine and PEG 4000 as a potential rapid release dosage form, Eur. J. Pharm. Biopharm. 53 (1) (2002) 125–132.

[4] D. voinovich, M. Moneghini, B. Perissutti, J. Filipovic-Grcic, J. Grabnar, preparation in high-shear mixer of sustained-release pellets by melt pelletisation, Int. J. Pharm. 203 (1–2) (2000) 235–244.

[5] D. Voinovich, M. Moneghini, B. Perissutti, E. Franceschinis, Melt pelletization in high shear mixer using a hydrophobic melt binder: influence of some apparatus and process variables, Eur. J. Pharm. Biopharm. 52 (3) (2001) 305–313.

[6] G.A. Lewis, D. Mathieu, R. Phan-Tan-Luu, Methods for non-standard designs, in: J. Swarbrick (Ed.), Pharmaceutical Experimental Design, Vol. 92, Marcel Dekker, New York, 1999.

[7] J. Nony, R. Phan-Tan-Luu, NEMRODW (New Efficient Tecnhnology for research using Optimal Design) software-L.P.R.A.I., Marseille 2002.

[8] V.G. Levich, Physicochemical Hydrodynamics, Prentice-Hall, Englewood Cliffs, NJ, 1962.

[9] M. Grassi, I. Colombo, R. Lapasin, Experimental determination of the theophylline diffusion coefficient in swollen sodium-alginate membranes, J. Control. Release 76 (2001) 93–105.

[10] M. Grassi, D. Voinovich, M. Moneghini, E. Franceschinis, B. Perissutti, J. Filipovic-Grcic, Preparation and evaluation of a melt pelletised paracetamol/stearic acid sustained release delivery system, J. Control. Release 88 (3) (2003) 381–391.

[11] M. Giona, Statistical analysis of anomalous transport phenomena in complex media, AIChE J. 37 (1991) 1249–1254.

[12] N. Peppas, Mathematical models for controlled release kinetics, in: R.S. Langer, D.L. Wise (Eds.), Medical Application of Controlled Release, Vol. I, CRC Press, Boca Raton, FL, 1984, p. 169.

[13] M.J. Abdekhodaie, Y.L. Cheng, Diffusional release of a dispersed solute from planar and spherical matrices into finite external volume, J. Control. Release 43 (1997) 175–182.

[14] M. Grassi, R. Lapasin, S. Pricl, The effect of drug dissolution on drug release from swelling polymeric matrices: mathematical modelling, Chem. Eng. Commun. 173 (1999) 147–173.

[15] Y.R. Byun, Y.K. Choi, S.Y. Jeong, Y.H. Kim, A model for diffusion and dissolution controlled release from dispersed polymeric matrix, J. Kor. Pharm. Sci. 20 (1990) 79–88.

[16] R. Gurny, E. Doelker, N.A. Peppas, Modelling of sustained release of water-soluble drugs from porous, hydrophobic polymers, Biomaterials 3 (1982) 27–32.

[17] N.A. Peppas, A model of dissolution-controlled solute release from porous drug-delivery polymeric systems, J. Biomed. Mater. Res. 17 (1983) 1079–1087.

[18] R.S. Harland, C. Dubernet, J.P. Benoît, N.A. Peppas, A model of dissolution-controlled, diffusional drug release from non-swellable polymeric microspheres, J. Control. Release 7 (1988) 207–215.

[19] S.V. Patankar, Numerical Heat Transfer and Fluid Flow, Hemisphere, New York, 1990.

[20] J. Crank, The Mathematics of Diffusion, 2nd Edition, Clarendon Press, Oxford, 1975.

[21] M. Grassi, I. Colombo, R. Lapasin, Drug release from an ensemble of swellable crosslinked polymer particles, J. Control. Release 68 (2000) 97–113.

[22] X. Huang, C.S. Brazel, On the importance and mechanisms of burst release in controlled drug delivery—a review, J. Control. Release 73 (2001) 121–136.

[23] P. Colombo, R. Bettini, N.A. Peppas, Observation of swelling process and diffusion front position during swelling in hydroxypropyl methyl cellulose (HPMC) matrices containing a soluble drug, J. Control. Release 61 (1999) 83–91.

[24] P. Colombo, R. Bettini, P. Santi, A. De Ascentiis, N.A. Peppas, Analysis of the swelling and release mechanisms from drug delivery systems with emphasis on drug solubility and water transport, J. Control. Release 39 (1996) 231–237.

[25] P. Colombo, R. Bettini, P. Santi, N.A. Peppas, Swellable matrices for controlled drug delivery: gel-layer behaviour, mechanisms and optimal performance, PSTT 3 (2000) 198–204.